High-resolution Time-independent Grid-based Forecast for M >= 5 Earthquakes in California

A. Helmstetter, Yan Y. Kagan, David D. Jackson

PostScript file created: November 20, 2007; time 1036 minutes

High-resolution time-independent grid-based forecast for $m \geq 5$ earthquakes in California

Agnès Helmstetter[1,2], Yan Y. Kagan[3] and David D. Jackson[3]

[1] Lamont-Doherty Earth Observatory, Columbia University, New York

[2] Now at LGIT, University Joseph Fourier, Grenoble, France

[3] Department of Earth and Space Sciences, University of California, Los Angeles

INTRODUCTION

We have developed time-independent forecasts for California assuming that small earthquakes can be used to map the distribution of large damaging earthquakes, as suggested by Kafka and Levin (2000). Indeed, large earthquakes often nucleate in areas that have a large density of small events.

We have first declustered the catalog to remove large fluctuations of seismic activity which do no represent the long-term average. We have then estimated the spatial density of seismicity using a kernel method to smooth the location of magnitude $m \geq 2$ earthquakes. Note that our model only predicts hypocenters, not rupture areas. Clearly, large earthquakes sometime propagate in areas with little seismicity, as observed for the 1857 earthquake that ruptured the southern section of the San Andreas fault, which is now mostly devoid of small earthquakes. Our model should thus be coupled with a fault model to forecast rupture areas for large earthquakes.

Our model is very similar to the time-independent forecasts of Helmstetter *et al.* (2006), which is in its turn an adaptation of the program by Kagan and Jackson (1994) to local modern catalogs. Compared with (Helmstetter *et al.*, 2006), we have extended our forecasts to all California, and done small changes in the method. We have slightly modified the declustering method. We have modified the estimation of the smoothing distance d_i used to estimate the spatial density of seismicity. Our new method is simpler and computationally more efficient, but gives very similar results. We have also estimated the completeness magnitude m_0 in each cell, and corrected our model to account for spatial variations of m_0.

We have developed two time-independent models for the RELM earthquake forecast testing (Kagan *et al.*, 2003; Schorlemmer *et al.*, 2005). The first one evaluates the expected rate of all $m \geq 5$ earthquakes, while the other one estimates the probability of independent events only. The two models have the same spatial distribution, but different total number of predicted events, and slightly different magnitude distributions.

Instead of the Gutenberg-Richter law (Gutenberg and Richter, 1944) with a uniform b-value of 1 used by Helmstetter et al. [2006], we use a tapered Gutenberg-Richter law with a corner magnitude $m_c = 8$, with $b = 0.95$ for the first model (all events) and $b = 0.89$ for the second model (estimated from independent events). We modify the magnitude distribution in the Geysers geothermal area, which has a much larger value $b \approx 2$ for $m \geq 3.3$.

EARTHQUAKE CATALOG AND DECLUSTERING

We use earthquakes of magnitude $m \geq 2$ in the Advanced National Seismic System (ANSS) catalog, in the time period from 1981/1/1 to 2005/8/23. We selected earthquakes within a rectangular area $30.55^\circ <$ latitude $< 43.95^\circ$ and $-126.35^\circ <$ longitude $< -112.15^\circ$, larger by 1° than the RELM testing area, to avoid finite region size effects.

In order to measure the time-independent earthquake rate, we need to decluster the catalog to remove large fluctuations of seismicity rate in space and time due to aftershock sequences. For that we used Reasenberg's (1985) declustering algorithm. The program CLUSTER2000 is available at http://quake.wr.usgs.gov/research/software. Reasenberg (1985) identified aftershocks by modeling an interaction zone around each earthquake. The spatial size of the interaction zone is based on an estimate of the stress redistribution following each earthquake. The temporal extent of the interaction zone is based on an Omori law decay of earthquake frequency following an event of a given magnitude. Two earthquakes are associated if their hypocentral and origin time difference are respectively less than the spatial and temporal extent of the dynamically modeled interaction zone for the first event (Reasenberg, 1985). We used the following parameters:

- $r_{\rm fact} = 8$ (number of crack radii surrounding each earthquake within which to consider linking a new event into cluster)
- $x_{\rm meff} = 2.00$ ("effective" lower magnitude cutoff for catalog)
- $x_{\rm k} = 0.50$ (increase of the lower magnitude cutoff during clusters: $x_{\rm meff} = x_{\rm meff} + x_k m$, where m is the magnitude of the largest event of the cluster)
- $p_1 = 0.95$ (probability of detecting the next clustered event, used to compute the look-ahead time τ)
- $\tau_{\rm min} = 1.0$ day (minimum value of the look-ahead time for building clusters, when the first event is not clustered)

- $\tau_{\max} = 5.0$ days (maximum value of look-ahead time for building clusters)
- minimum cluster size of 5 events.

We modified the expression of the interaction distance in Reasenberg's code. We use $r = 0.01 \times 10^{0.5m}$ km, as suggested by Wells and Coppersmith (1994) for the scaling of rupture length with magnitude in California, instead of $r = 0.011 \times 10^{0.4m}$ and $r < 30$ km in Reasenberg's algorithm.

The resulting declustered catalog has 81659 "independent events" ("mainshocks" and "background" events), and 75545 "dependent events" ("foreshocks" and "aftershocks"). The parameters of the declustering algorithm were adjusted to remove large fluctuations of seismic activity in space and time. Clearly, the resulting declustered catalog is still clustered in space and time, as can be seen from the distribution of interevent times, which presents a deviation from an exponential distribution at short times. However, this residual clustering occurs at small space and time scales. Therefore, the density measured from this declustered catalog over large scales gives a good estimation of the long-term spatial distribution of seismicity. The declustered catalog is shown in Figure 1.

SPATIAL DISTRIBUTION OF SEISMICITY

We estimate the density of seismicity in each cell by smoothing the location of each earthquake i with an isotropic adaptive kernel $K_{d_i}(\vec{r})$. We tested two choices for $K_d(\vec{r})$, either a power-law

$$K_d(\vec{r}) = \frac{C(d)}{(|\vec{r}|^2 + d^2)^{1.5}}\,, \qquad (1)$$

or a Gaussian

$$K_d(\vec{r}) = C'(d)\ \exp\left[-\frac{|\vec{r}|^2}{2\,d^2}\right]\,, \qquad (2)$$

where d is the smoothing distance, and $C(d)$ and $C'(d)$ are normalizing factors, so that the integral of $K_d(\vec{r})$ over an infinite area equals 1.

We measure the smoothing distance d_i associated with earthquake i as the horizontal distance between event i and the n_v^{th} closest neighbor. The number of neighbors, n_v, is an adjustable parameter, estimated by optimizing the forecasts. We impose $d_i > 0.5$ km to account for location accuracy. The kernel bandwidth d_i thus decreases if the density of seismicity at the location $\vec{r_i}$ of this earthquake increases, so that we have a better resolution (smaller d_i) where the density is higher.

The density at any point $\vec{r}$ is then estimated by

$$\mu(\vec{r})\ = \sum_{i=1}^{N} K_{d_i}(\vec{r} - \vec{r_i})\,. \qquad (3)$$

Our forecasts are given as an average number of events in each cell of 0.1°. The density defined by (3) has fluctuations at scales smaller than the grid resolution. Therefore, we need to integrate $\mu(\vec{r})$ defined by (3) over each cell to obtain the seismicity rate in this cell.

CORRECTING FOR CATALOG INCOMPLETENESS

We have used events with $m \geq 2$ to estimate the spatial distribution of seismicity. Unfortunately, the catalog is not complete everywhere at this magnitude level. Moreover, two regions, one south of 32° N (Mexico), and one west of 124.5° W (Mendocino area), have a much larger completeness magnitude (up to ≈ 4), and have also a high rate of large earthquakes. In order to correct for catalog incompleteness, we have estimated the completeness magnitude m_0 in each cell from the magnitude distribution.

We can estimate the magnitude distribution $P_m(\vec{r}, m)$ at point $\vec{r}$ using the same kernel method as described above to estimate the density $\mu(\vec{r})$. We now smooth both the locations and magnitudes of all earthquakes using

$$P_m(\vec{r}, m)\ = \sum_{i=1}^{N} K_{d_i}(\vec{r} - \vec{r_i})\, G_h(m - m_i)\,, \qquad (4)$$

where $G_h(m)$ is a Gaussian function of mean m and width h. The kernel width h is fixed to 15 km. We then integrate $P_m(\vec{r}, m)$ over each cell to get the magnitude distribution in this cell.

The simplest method to estimate the completeness magnitude is to define m_0 as the maxima of the smoothed magnitude distribution in each cell. Using this method, we obtain large small-scale fluctuations of m_0, which are probably non-physical. The completeness magnitude should be relatively smooth at scales smaller than the typical distance between seismic stations. Therefore we smooth the completeness magnitude m_0 using a Gaussian filter with a standard deviation of 15 km. The result is shown in Figure 2. The central part of the testing area has $m_0 \approx 2$. The

completeness magnitude is much larger, up to $m_0 = 4$, close to the boundaries of the testing areas, especially in the Mendocino area and in Mexico. Note that a completely different method to estimate m_0 has been proposed by Bachmann *et al.* (2005). Instead of using the magnitude distribution to estimate m_0, they use the spatial distribution of seismic stations and the detection characteristics of each station to map m_0.

The forecasted rate of events with $m \geq m_{\min}$ in each cell can then be corrected from spatial variations of m_0 assuming that the magnitudes obey the Gutenberg-Richter law (Gutenberg and Richter, 1944) with $b = 1$

$$\mu'(\vec{r}) = \mu(\vec{r})\, 10^{m_0(\vec{r}) - m_{\min}} . \quad (5)$$

LIKELIHOOD, PROBABILITY GAIN, AND MODEL OPTIMIZATION

We estimate the parameter n_v (the number of neighbors, used to compute the smoothing distance d_i in (3)) by optimizing the likelihood of the model. We use two different data sets to build the model $\mu'(i_x, i_y)$ and to test it. We evaluate the performance of the forecasts by computing the likelihood of the model. In this section, we are interested only in the spatial distribution of seismicity. We do not consider the magnitude distribution of target events, or the expected number of events. Therefore, we compute the normalized density $\mu^*(i_x, i_y)$ in each cell (i_x, i_y) using

$$\mu^*(i_x, i_y) = \frac{\mu'(i_x, i_y)\, N_t}{\sum_{i'_x=1}^{N_x} \sum_{i'_y=1}^{N_y} \mu(i'_x, i'_y)} , \quad (6)$$

where N_x and N_y are the total numbers of columns and rows, and N_t is the number of target events. The expected number of events for the model μ^* thus equals the observed number N_t.

The log-likelihood of the model is given by

$$L = \sum_{i_x=1}^{N_x} \sum_{i_y=1}^{N_y} \log p\,[\,\mu^*(i_x, i_y), n\,] , \quad (7)$$

where n is the number of events that occurred in the cell (i_x, i_y).

Assuming a Poisson process, the probability $p[\mu^*(i_x, i_y), n]$ of having n events in the cell (i_x, i_y) is given by

$$p[\mu^*(i_x, i_y), n] = [\mu^*(i_x, i_y)]^n \, \frac{\exp[-\mu^*(i_x, i_y)]}{n!} , \quad (8)$$

We have tried different values of the minimum magnitude, both for the input catalog (used to measure μ) and for the target events (used to test the model). We use the same catalog for the input and target events, but different time intervals or magnitude intervals, so that earthquakes used to estimate μ are not used as target events to test the model. We evaluate the performance of our forecasts using the probability gain per earthquake of the model relative to a model with a uniform density

$$G = \exp\left(\frac{L - L_{\text{unif}}}{N_t}\right) , \quad (9)$$

where L_{unif} is the log-likelihood for a uniform model.

The results are summarized in Table 1. Figure 3 shows the density for model #2 in Table 1. The power-law kernel (2) gives a slightly larger likelihood than the Gaussian (1) (see models #1 and #2 in Table 1).

The probability gain does not change significantly with the minimum magnitude of target events for $3 \leq m_{\min} \leq 5.5$ (see models #2-7). This suggests that small and large earthquakes have about the same spatial distribution, i.e., that the magnitude distribution is relatively uniform in space, at scales larger than the cell size of ≈ 10 km.

In contrast, the probability gain decreases continuously with the minimum magnitude of input data, as shown in models #8-20 in Table 1. The probability gain per earthquake, for target earthquakes with $m \geq 5$, decreases from $G = 3.0$ for $m_{\min} = 2$, to $G = 1.2$ for $m_{\min} = 5$. G decreases with $m_{\min}$ because the number of events used to compute μ decreases, thus the resolution of the model decreases.

Model #21 in Table 1 uses all the available input data, from 1981/1/1 to 2005/8/23, in order to estimate μ. When tested on $m \geq 3$ target earthquakes since 1996, this model gives a larger gain than model #2, which used only 1981-1996 data to build the model. The increase of G between $G = 4.8$ for model #2 and $G = 7.1$ for model #21 may be partly due to the increase of the number of input events. But it's mainly due to the fact that we use (in part) the same data to build the model and to test it. Our final model (our forecast for the next 5 yrs) is model #21 in Table 1, which uses all available data.

CONCENTRATION PLOT

Another tool to test a model is the "concentration plot", which compares the observed and expected

number of events as a function of the modeled density μ. The concentration plot for model #2 is shown in Figure 4. The upper plot shows the cumulative number of events as a function of the value of μ in the cells where these events occur. The lower plot shows the probability density function (obtained by taking the derivative of the curves in Figure 4a): the observed and expected number of events within each interval of μ-values. A model is incorrect if there is a significant deviation between the observed and modeled distributions. If the observed distribution is shifted to the right compared to the expected one, the model is too smooth. In our case, the observed curves are slightly to the left of the model, which means that our model is too "localized": there are more observed events in the regions of low modeled probability μ that expected.

A model is better than another one if the observed distribution in the concentration plot is shifted toward larger values of μ. The μ values in Figure 4 have been normalized so that the sum over the testing area equals 1. For comparison, a uniform model would have a density $\mu_{\rm unif} = 1/N_c = 1.3 \times 10^{-4}$ (where $N_c = 7642$ is the number of cells in the testing area). As shown in Figure 4, most events (79%) occur within cells where the modeled density is larger than the average $\mu_{\rm unif}$. For this model, the average value of the density at the location of a target earthquake is 18 times larger than the average value.

MAGNITUDE DISTRIBUTION

We assume for simplicity that the magnitude distribution obeys a tapered Gutenberg-Richter law (Gutenberg and Richter, 1944) with a uniform b-value and corner magnitude m_c. Specifically, we assume that the cumulative magnitude distribution has the form

$$P(m) = 10^{-b(m-m_{\rm min})} \exp\left[10^{1.5(m_{\rm min}-m_c)}] - 10^{1.5(m-m_c)}\right] , \quad (10)$$

with a minimum magnitude $m_{\rm min} = 4.95$, and a corner magnitude $m_c = 8$, as suggested by Bird and Kagan (2004) for continental transform fault boundaries. The exponential factor in (10) describes a falloff of the distribution of seismic moments $M \sim 10^{1.5m}$.

We use the catalog provided by RELM (available at http://proto-testing.ethz.ch/downloads/ANSS.catalog.dat), because it uses the same magnitude type and declustering method as will be used for the RELM tests. This catalog contains all events in the ANSS catalog in California with $m \geq 3$, between 1984 and 2004, and gives the independence probability p_i for each earthquake.

We have measured the b-value using the likelihood method (Aki, 1965)

$$b = \frac{1}{\log(10)(< m > -m_{\rm min})} . \quad (11)$$

For the non-declustered catalog, this gives $b = 0.95$. In order to estimate the b-value of independent events, we have measured the average magnitude $< m >$ in (11) by selecting all events in the RELM catalog within the testing area, with $m \geq 4.95$, and weighting each earthquake by its independence probability. This gives $b = 0.89$, with a number of independent events of 93. The declustering procedure slightly decreases the b-value, because it removes preferentially small events. The cumulative magnitude distribution for the non-declustered catalog is shown in Figure 5.

There is however a region, the Geysers in Northern California (lat $\approx 38.8°$ N, and lon $\approx 128.8^0$ W), which has an unusual magnitude distribution. It has many small $m \geq 2$ events and a very large b-value. These earthquakes are induced by the geothermal activity in this area. If we assume that the magnitude distribution in this region obeys the Gutenberg-Richter law with $b = 0.89$, this gives a very large expected rate of $m \geq 5$ earthquakes, close to the largest value in all California, while the largest event has $m = 4.7$ (see Figure 3).

We have thus modified the magnitude distribution in this area (for $-128.9° < \text{lon} < -128.7°$, and $38.7° < \text{lat} < 38.9°$). We have fitted the magnitude distribution by the Gutenberg-Richter law, selecting all events with $m \geq 3.3$ in the RELM declustered catalog. The maximum likelihood method gives $b = 1.94$. We use the same corner magnitude $m_c = 8$ in this region as everywhere else. For smaller events with $m < 3$, the magnitude distribution has a more usual b-value close to 1.

The cumulative magnitude distribution for the Geysers is shown in Figure 5. We have used this fit to estimate the expected rate of $m \geq 5$ earthquakes at the Geysers, from the modeled density of $m \geq 2$ events. This correction decreases the expected rate of $m \geq 5$ events by a factor 80 at the Geysers compared to the model with a uniform magnitude distribution with $b = 0.89$ (see Figure 5). The difference further increases for larger target events. We checked that other geothermal or volcanic areas (Mammoth Lakes, Coso, Salton Sea) have a magnitude distribution close to the global distribution for California. Geothermal

activity is thus not the sole cause of anomalous magnitude distribution at the Geysers.

The corrected density of $m \geq 5$ events is shown in Figure 6. Compared to Figure 3, the dark spot at the Geysers has disappeared. The differences between Figures 3 and 6 are the change in $P(m)$ for the Geysers and the time window used to select input events. Figure 3 compares forecasted rate using 1981-1996 data with earthquakes that occurred since 1996. It is thus a pseudo-real time test of the model. Figure 6 is our final forecast, which uses all available data between 1981/1/1 and 2005/8/23. The fact that the 2 models are very similar is encouraging. This shows that the spatial density does not change significantly with time.

EXPECTED NUMBER OF EVENTS

We have estimated the total expected number of target events by counting the number of $m > 4.95$ earthquakes in the RELM catalog, which occurred within the testing area, during the time window 1984-2004. We have removed 9 $m \geq 5$ events from this catalog that are explosions. This gives a total number of 7.38 earthquakes per year.

In order to estimate the rate of independent events, we have weighted each earthquake by its independence probability. This gives an average number of 4.41 events per year. We then estimate the expected number of events per year within each space-time-magnitude bin according to

$$E(i_x, i_y, i_m) = N_0 \, \mu_0(i_x, i_y) \, P(i_m) \, , \qquad (12)$$

where N_0 is the expected number of target events per year in the testing area, μ_0 is equal to the spatial distribution μ, normalized so that the sum of μ_0 in the testing area equals 1, and $P(i_m)$ is the expected number of events within the magnitude bin i_m, estimated from (10). For the first model, we use $N_0 = 7.38$ and $b = 0.95$. For the second model (to forecast independent $m \geq 5$ events), we use $N_0 = 4.41$ and $b = 0.89$.

CONCLUSION

We have developed a time-independent forecast for California, by smoothing seismicity. We have shown that including small $m \geq 2$ events to predict larger $m \geq 5$ earthquakes significantly improves the performance of the model. In contrast, the performance of our model does not depend on the minimum magnitude of target events: our model predicts as well $m \geq 3$ and $m \geq 5.5$ events. This suggests that large earthquakes have the same spatial distribution as smaller ones, and justifies our use of small earthquakes to estimate the probability of larger ones.

We have taken into account spatial variations of the completeness magnitude. We have also modified the magnitude distribution in the Geysers geothermal area, which has a very unusually large b-value. This correction is rather artificial, and in the future we would like to use a more systematic approach to estimate the magnitude distribution in each cell.

Because there are not enough large historical earthquakes in California, we cannot measure the corner magnitude m_c (magnitude at which the magnitude distribution deviates from a pure Gutenberg-Richter law). We thus use a uniform value $m_c = 8$, as suggested by Bird and Kagan (2004) for continental transform fault boundaries.

Some would argue that this corner magnitude may not hold for all of California, because there are few long enough faults in California which could produce a $m = 8$ earthquake. However, it is becoming increasingly apparent that fault length is not a reliable barrier to earthquake growth: Gabrielov *et al.* (1996) show that plate geometry cannot be stable on a deforming Earth, and of course the faults we see today were not always there. Black *et al.* (2004) present evidence that southern California earthquakes commonly break the boundaries of geologically mapped faults. Also, the Denali 2002 M7.9 earthquake in Alaska started at a small unknown thrust fault and then proceeded to rupture strike-slip Denali fault, then rupturing Totschunda fault (Rowe *et al.* 2004).

In addition to the epicenter, seismic hazard estimation also requires the specification of the fault plane. Kagan and Jackson (1994) have developed a method to forecast the orientation of the fault plane, by smoothing the focal mechanisms of past $m \geq 5.5$ earthquakes. As for forecasting epicenters, it may be useful to include small earthquakes in the forecasts, in order to improve the resolution. Alternatively, our model could be coupled with fault models to predict the rupture geometry of very large earthquakes, which are likely to break a known fault.

Acknowledgments. We acknowledge the Advanced National Seismic System for the earthquake catalog. Part of this work was done while one of the authors (AH) was at the KITP in Santa Barbara. This work is partially supported by NSF-EAR02-30429, NSF-PHY99-0794, NSF-EAR03-37226, NSF-EAR-0409890, by the Southern Cal-

ifornia Earthquake Center (SCEC), by the James S. McDonnell Foundation 21st century scientist award/studying complex system, and by the Brinson Foundation. SCEC is funded by NSF Cooperative Agreement EAR-0106924 and USGS Cooperative Agreement 02HQAG0008. The SCEC contribution number for this paper is 983.

References

Aki, K. (1965), Maximum likelihood estimate of b in the formula $logN = a - bM$ and its confidence limits, *Bulletin of the Earthquake Research Institute* **43**, 237-239.

Bachmann, C., D. Schorlemmer, J. Woessner, and S. Wiemer (2005). Probabilistic estimates of monitoring completeness of seismic networks, *Eos Transactions of the American Geophysical Union*, **86**(52), Fall Meeting Supplement, Abstract S33A-0304.

Bird, P., and Y. Y. Kagan (2004). Plate-tectonic analysis of shallow seismicity: Apparent boundary width, beta, corner magnitude, coupled lithosphere thickness, and coupling in seven tectonic settings, *Bulletin of the Seismological Society of America* **94**(6), 2380-2399.

Black, N., D. D. Jackson, and T. Rockwell (2004). Maximum Magnitude in Relation to Mapped Fault Length and Fault Rupture, *Eos Transactions of the American Geophysical Union*, **85**(47), Fall Meeting Supplement, Abstract S41A-0922.

Gabrielov, A., V. Keilis-Borok, and D. D. Jackson (1996). Geometric incompatibility in a fault system, *Proceedings of the National Academy of Sciences of the United States of America* **93**, 3838-3842.

Gutenberg, B., and C.F. Richter (1944). Frequency of earthquakes in California, *Bull. seism. Soc. Am.*, **142**, 185188.

Helmstetter, A., Y. Y. Kagan, and D. D. Jackson (2006). Comparison of short-term and time-independent earthquake forecast models for southern California, *Bulletin of the Seismological Society of America* **96**(1), 90-106.

Kafka, A. L. and S. Z. Levin (2000). Does the spatial distribution of smaller earthquakes delineate areas where larger earthquakes are likely to occur? *Bulletin of the Seismological Society of America* **90**, 724-738.

Kagan, Y. Y. and D. D. Jackson (1994). Long-term probabilistic forecasting of earthquakes, *Journal of Geophysical Research* **99**, 13,685-13,700.

Kagan, Y. Y., D. D. Jackson, D. Schorlemmer, and M. Gerstenberger (2003). Testing hypotheses of earthquake occurrence, *Eos Transactions of the American Geophysical Union*, **84**(47), Fall Meeting Supplement, Abstract S31G-01.

Reasenberg, P. (1985). Second-order moment of Central California seismicity, 1969-1982, *Journal of Geophysical Research* **90**, 5479-5495.

Rowe, C., D. Christensen, and G. Carver (2004). Preface to the issue dedicated to the 2002 Denali fault earthquake sequence, *Bulletin of the Seismological Society of America* **94**(6B), S1-S4.

Schorlemmer D., M. Gerstenberger, S. Wiemer, and D. D. Jackson (2005). Earthquake likelihood model testing, in preparation, preliminary draft available at http://moho.ess.ucla.edu/∼kagan/sjg.pdf.

Wells, D. L. and K. J. Coppersmith (1994). New empirical relationships among magnitude, rupture length, rupture width, rupture area, and surface displacement, *Bulletin of the Seismological Society of America* **84**, 974-1002.

Agnès Helmstetter, Lamont-Doherty Earth Observatory, 61 Rte 9W, Palisades, NY 10964 (e-mail: agnes@ldeo.columbia.edu)

Yan Y. Kagan, Department of Earth and Space Sciences, University of California, Los Angeles, California 90095-1567. (e-mail: ykagan@ucla.edu)

David D. Jackson, Department of Earth and Space Sciences, University of California, Los Angeles, California 90095-1567. (e-mail: djackson@ucla.edu)

This preprint was prepared with AGU's LaTeX macros v5.01. File HKL˙SRL2006˙final formatted November 20, 2007.

Table 1. Time interval $[t_1 \;\; t_2]$ and minimum magnitude $m_{\min}$ used to select input events and target earthquakes. Input events are used to compute μ. Target events are used to evaluate the log-likelihood L (7) and the probability gain per earthquake G (9). The smoothing parameter n_v is adjusted to maximize L. The second column specifies the kernel function used to smooth earthquake locations, either a power-law ('pl') or a Gaussian ('gs').

#	K	t_1	t_2	$m_{\min}$	N	t_1	t_2	$m_{\min}$	N_t	L	G	n_v
		Input catalog				Target catalog						
1	gs	1981/1/1	1996/1/1	2.	52651	1996/1/1	2005/8/23	3.	2747	-4145.	4.78	2
2	pl	1981/1/1	1996/1/1	2.	52651	1996/1/1	2005/8/23	3.	2747	-4121.	4.83	2
3	pl	1981/1/1	1996/1/1	2.	52651	1996/1/1	2005/8/23	3.5	852	-1903.	4.33	2
4	pl	1981/1/1	1996/1/1	2.	52651	1996/1/1	2005/8/23	4.	288	-918.	3.88	2
5	pl	1981/1/1	1996/1/1	2.	52651	1996/1/1	2005/8/23	4.5	78	-358.	2.99	2
6	pl	1981/1/1	1996/1/1	2.	52651	1996/1/1	2005/8/23	5.	33	-178.	2.98	2
7	pl	1981/1/1	1996/1/1	2.	52651	1996/1/1	2005/8/23	5.5	8	-52.	4.15	2
8	pl	1981/1/1	1996/1/1	2.5	19215	1996/1/1	2005/8/23	3	. 2747	-4125.	4.82	2
9	pl	1981/1/1	1996/1/1	3.	6011	1996/1/1	2005/8/23	3.	2747	-4284.	4.55	2
10	pl	1981/1/1	1996/1/1	3.5	1839	1996/1/1	2005/8/23	3.	2747	-4835.	3.72	2
11	pl	1981/1/1	1996/1/1	4.	611	1996/1/1	2005/8/23	3.	2747	-5694.	2.72	2
12	pl	1981/1/1	1996/1/1	4.5	201	1996/1/1	2005/8/23	3.	2747	-6686.	1.89	1
13	pl	1981/1/1	1996/1/1	5.	78	1996/1/1	2005/8/23	3.	2747	-8009.	1.17	1
14	pl	1981/1/1	1996/1/1	2.	52651	1996/1/1	2005/8/23	5.	33	-178.	2.98	2
15	pl	1981/1/1	1996/1/1	2.5	19215	1996/1/1	2005/8/23	5.	33	-179.	2.90	6
16	pl	1981/1/1	1996/1/1	3.	6011	1996/1/1	2005/8/23	5.	33	-181.	2.67	4
17	pl	1981/1/1	1996/1/1	3.5	1839	1996/1/1	2005/8/23	5.	33	-185.	2.40	2
18	pl	1981/1/1	1996/1/1	4.	611	1996/1/1	2005/8/23	5.	33	-191.	1.96	2
19	pl	1981/1/1	1996/1/1	4.5	201	1996/1/1	2005/8/23	5.	33	-204.	1.35	4
20	pl	1981/1/1	1996/1/1	5.	78	1996/1/1	2005/8/23	5.	31	-208.	1.19	4
21	pl	1981/1/1	2005/8/23	2.	81659	1996/1/1	2005/8/23	3.	2747	-3069.	7.08	6

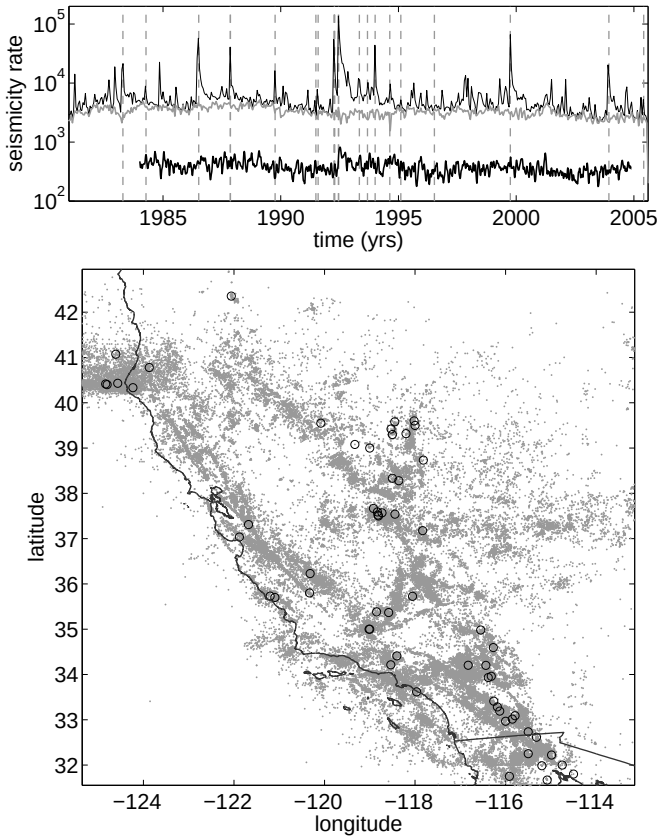

Figure 1. (a) Seismicity rate for the ANSS catalog (thin black line on top), for our declustered catalog (gray line), and for the RELM declustered catalog (see http://proto-testing.ethz.ch/downloads) (solid black line). The seismicity rate for the RELM catalog is about 10 time smaller due to the larger threshold magnitude ($m_{\min} = 3$ for RELM catalog but $m_{\min} = 2$ for our catalog). It increases by a factor of about 2 at the time of Landers 1992/6/28, $m = 7.3$ earthquake, showing that this catalog is not completely declustered. Vertical dashed lines show the time of each $m \geq 6$ earthquake. (b) Seismicity map for our declustered catalog (dots), and location of $m \geq 6$ earthquakes (circles).

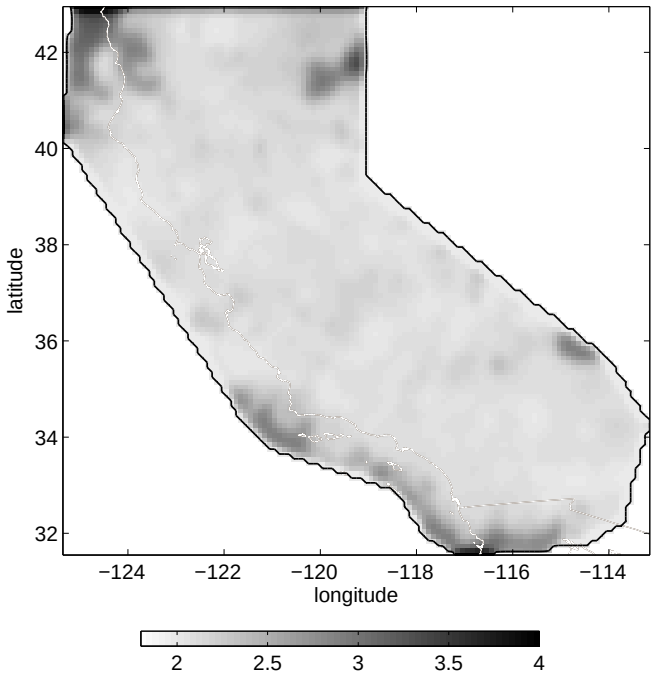

Figure 2. Completeness magnitude m_0, estimated by the maxima of the magnitude distribution in each cell, using declustered $m \geq 2$ earthquakes from 1981/1/1 to 2005/8/23.

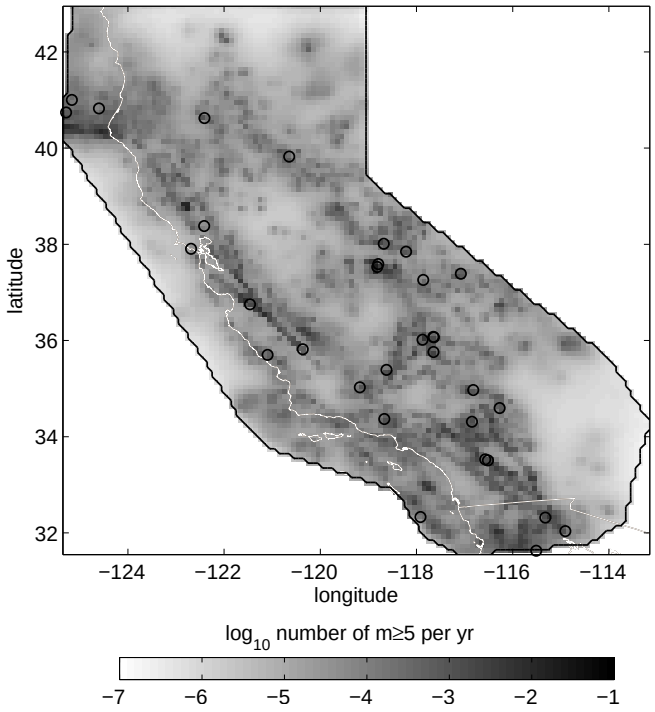

Figure 3. Forecasted seismicity rate (expected number of $m > 4.95$ events per year in each cell) for model #2 in Table 1, using a power-law kernel to smooth the location of $m \geq 2$ earthquakes from 1981 to 1996. Circles are $m \geq 5$ earthquakes that occurred between 1996/1/1 and 2005/8/23.

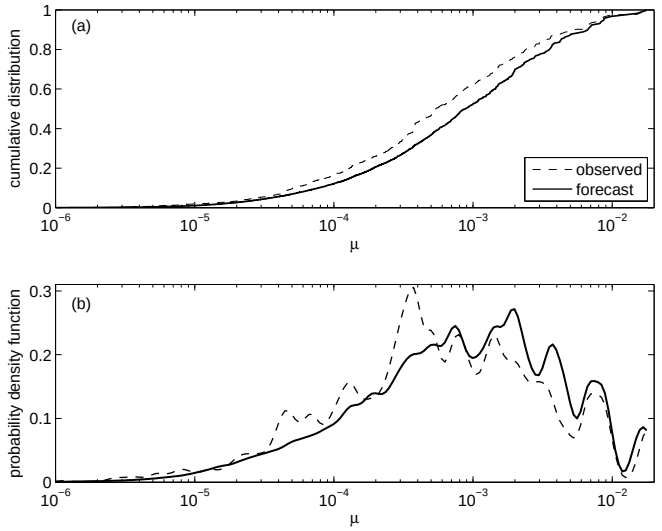

Figure 4. Concentration plot for model #2 in Table 1, shown in Figure 3. The solid line is the expected number of events as a function of the modeled density μ, and the dashed line is the observed number. (a) Cumulative distribution: number of earthquakes that occur in a cell with $\mu^*(i_x, i_y) < \mu$. (b) Probability density function.

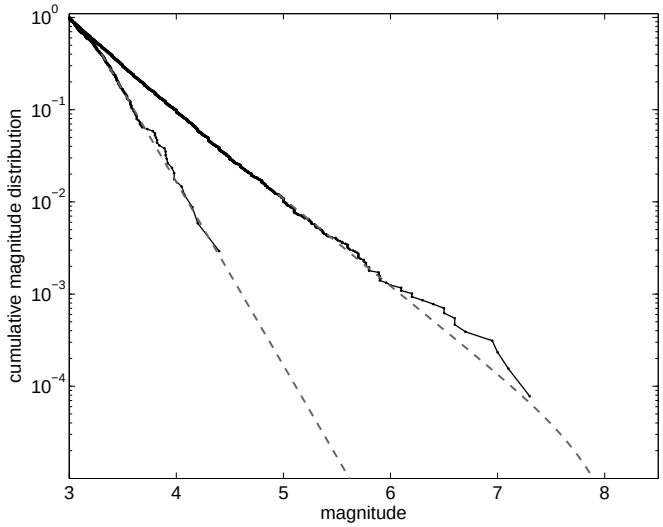

Figure 5. Cumulative magnitude distribution, for all earthquakes within the testing area between 1984 and 2004 (solid line with dots), and fit by (10) (dashed line) with $b = 0.93$ for $m \geq 5$. The lower curves are for the Geysers geothermal area. The dashed line is a fit by (10) with $b = 1.99$ for $m \geq 3.3$.

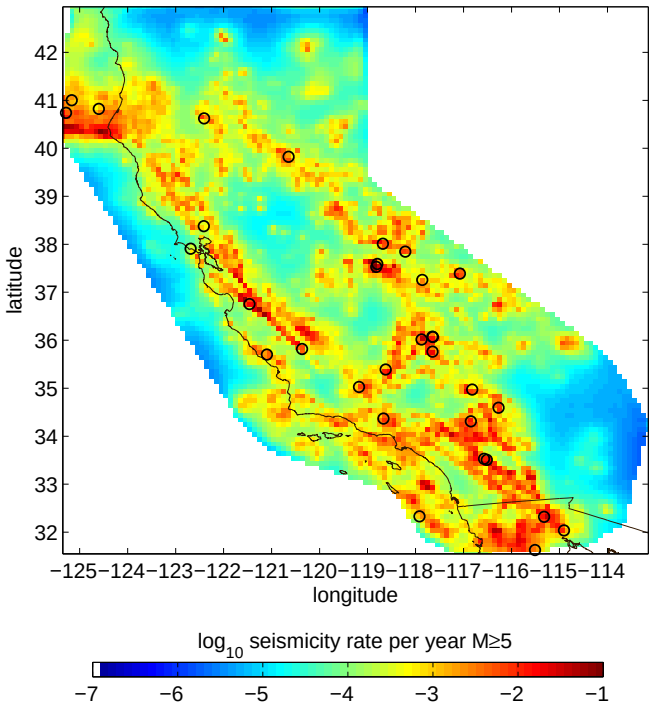

Figure 6. Forecasted seismicity rate (expected number of $m > 4.95$ events per year in each cell) for model #21 in Table 1, using a power-law kernel to smooth the location of $m \geq 2$ earthquakes from 1981 to 2005. Circles are $m \geq 5$ earthquakes that occurred between 1996/1/1 and 2005/8/23.